# (μ-Oxo)diiron Complexes of Gated Glyoximes. Structural Changes Accompanying Ligation Trans to the Oxo Bridge

**Isak Vernik and Dennis V. Stynes***

Department of Chemistry, York University, North York, Ontario, Canada M3J 1P3

*Received June 28, 1995*[⊗]

Structures of new low-spin oxo-bridged complexes of bis[(diphenylboryl)dimethylglyoximato]iron, Fe((DMG)-$BPh_2)_2$, are reported. The pentacoordinate complex, **1** = $[Fe((DMG)BPh_2)_2]_2O$, contains a bent Fe−O−Fe bridge (166.0°) with the irons each displaced 0.3 Å out of the $N_4$ planes toward the oxo ligand. The Fe−μ-O bond length (1.7097(10) Å) is the shortest yet reported. Both axial phenyl groups are directed to the trans face, creating a superstructure which is collapsed around the vacant binding site. In the butylamine derivative, **2** = $[(BuNH_2)$-$Fe((DMG)BPh_2)_2)]_2O$, the Fe−O−Fe bridge is linear (178.6°) with iron in the $N_4$ plane and Fe−O bond lengths of 1.766(6) Å. The $BuNH_2$ ligand is sandwiched between the axial phenyl groups in intimate contact with them. Structural changes accompanying ligation and their consequences are compared with those in heme systems. Crystal data for **1**: orthorhombic, *Pnna*, $a = 17.440(3)$ Å, $b = 21.381(4)$ Å, $c = 16.896(3)$ Å, $V = 6300(2)$ Å$^3$, $Z = 4$, $R = 0.068$. Crystal data for **2** ($CHCl_3$ disolvate): triclinic, $P\bar{1}$, $a = 13.445(3)$ Å, $b = 14.525(4)$ Å, $c = 23.877(6)$ Å, $\alpha = 96.01°$, $\beta = 92.61°$, $\gamma = 117.40(1)°$, $V = 4094(2)$ Å$^3$, $Z = 2$, $R = 0.086$.

## Introduction

The Fe−O−Fe (μ-oxo)diiron unit is a common structural feature of the chemistry and biochemistry of Fe(III).[1] It is best known in oxo-bridged hemes[2] and Schiff base complexes[3] (Fe-(salen)) which exist exclusively as pentacoordinate species with antiferromagnetically coupled high-spin Fe(III)'s. A large number of multibridged diiron complexes (all high-spin) in which the oxo bridge is supported by carboxylate and other bridging ligands have also been described.[4] The phthalocyanines are the only example reported to date involving six-coordinate low-spin (μ-oxo)diiron complexes.[5]

The borylated dioximes[6] $Fe((DMG)BR_2)_2$ provide a strong in-plane ligand field[7] favoring an inert low-spin six-coordinate environment for Fe(II) and Fe(III) derivatives. The chemistry of divalent $Fe((DMG)BF_2)_2$ complexes is extensively developed.[6a,b] Some iron(III) complexes including the low-spin Fe-$((DMG)BF_2)Cl_2$ and strongly oxidizing μ-oxo Fe(III) derivatives were described.[6c,d] Attempts to obtain suitable crystals of μ-oxo $Fe((DMG)BF_2)_2$ complexes for structural characterization have been frustrated by their low solubility and slow spontaneous reduction to Fe(II).

We therefore turned our attention to the $Fe((DMG)BPh_2)_2$ system.[6e−h] In this system, facile movement of boron-linked phenyl groups from axial to equatorial sites occurs via the conformational dynamics of the two boroximato chelate rings. This feature contrasts with the greater rigidity of superstructured hemes[8] and the fixed orientation of the pickets in picket fence porphyrins.[8c] Thus the term "gated" glyoximes was coined for these complexes.[6e] The energetics of interaction between axially directed phenyl groups and a variety of substrates positioned in contact with them have been measured in the Fe(II) derivatives.[6g] In the μ-oxo complexes both axial phenyls are constrained to the distal face (trans to the oxo group), where they create a cyclophane-like cavity surrounding the trans binding site. We report structural data for two μ-oxo derivatives of the $BPh_2$ system here. Ligational equilibria and paramagnetic NMR data for a wide variety of axial ligated derivatives are presented separately.[6i]

## Experimental Section

The $Fe((DMG)BPh_2)_2(CH_3CN)_2$ starting material was prepared as described elsewhere.[6h] Solvents were dried over molecular sieves (3 Å). $^1$H NMR spectra were recorded on a Bruker ARX 400 MHz spectrometer. Solution magnetic moments were determined in $CDCl_3$

[⊗] Abstract published in *Advance ACS Abstracts,* March 1, 1996.

(1) (a) Murray, K. S. *Coord. Chem. Rev.* **1974**, *12*, 1−35. (b) Kurtz, D. M. *Chem. Rev.* **1990**, *90*, 585−606. (c) Vincent, J. B.; Olivier-Lilley, G. L.; Averill, B. A. *Chem. Rev.* **1990**, *90*, 1447−1467. (d) Haselhorst, G.; Wieghardt, K.; Keller, S.; Schrader, B. *Inorg. Chem.* **1993**, *32*, 520−525.

(2) (a) Hoffman, A. B.; Collins, D. M.; Day, V. W.; Fleischer, E. B.; Srivastava, T. S.; Hoard, J. L. *J. Am. Chem. Soc.* **1972**, *94*, 3620−3626. (b) Landrum, J. T.; Grimmett, D.; Haller, K. J.; Scheidt, W. R.; Reed, C. A. *J. Am. Chem. Soc.* **1981**, *103*, 2640−2650.

(3) (a) Mukherjee, R. N.; Stack, T. D. P.; Holm, R. H. *J. Am. Chem. Soc.* **1988**, *110*, 1850−1861. (b) Davies, J. E.; Gatehouse, B. M. *Acta Crystallogr.* **1973**, *B29*, 1934. (c) Corazza, F.; Floriani, C.; Zehnder, M. *J. Chem. Soc., Dalton Trans.* **1987**, 709.

(4) Gorun, S. M.; Lippard, S. J. *Inorg. Chem.* **1991**, *30*, 1625−1630.

(5) (a) Ercolani, C.; Gardini, M.; Murray, K. S.; Pennesi, G.; Rossi, G.; Zwack, P. R. *Inorg. Chem.* **1987**, *26*, 3539−3543. (b) Ercolani, C.; Monacelli, F.; Dzunga, S.; Goedken, V. L.; Pennesi, G.; Rossi, G. *J. Chem. Soc., Dalton Trans.* **1991**, 1309. (c) Sievertsen, S.; Murray, K. S.; Moubaraki, B.; Berry, K. J.; Korbatieh, Y.; Cashion, J. D.; Brown, L. J.; Homborg, H.; *Z. Anorg. Allg. Chem.* **1994**, *620*, 1203−1212.

(6) (a) Thompson, D. W.; Stynes, D. V. *Inorg. Chem.* **1990**, *29*, 3815−3822. (b) Thompson, D. W.; Stynes, D. V. *Inorg. Chem.* **1991**, *30*, 636−640. (c) Thompson, D. W.; Noglik, H.; Stynes, D. V. *Inorg. Chem.* **1991**, *30*, 4567−4571. (d) Noglik, H.; Thompson, D. W.; Stynes, D. V. *Inorg. Chem.* **1991**, *30*, 4571−4575. (e) Stynes, D. V.; Leznoff, D.; de Silva, D. G. A. H. *Inorg. Chem.* **1993**, *32*, 3989−3990. (f) Impey, G. A.; Stynes, D. V. *J. Am. Chem. Soc.* **1993**, *115*, 7868−7869. (g) Stynes, D. V. *Inorg. Chem.* **1994**, *33*, 5022−5029. (h) de Silva, D. G. A. H; Leznoff, D. B.; Impey, G. A.; Vernik, I.; Jin, Z.; Stynes, D. V. *Inorg. Chem.* **1995**, *34*, 4015−4025. (i) Vernik, I.; Stynes, D. V. *Inorg. Chem.* **1996**, *35*, 2011−2018.

(7) The $Fe((DMG)BR_2)_2$ systems contain a 14 membered macrocyclic ring. Hemes, phthalocyanines, and Busch cyclidene macrocycles[18] are all 16-membered rings.

(8) (a) Traylor, T. G.; Tsuchiya, S.; Campbell, D.; Mitchell, M.; Stynes, D. V.; Koga, N. *J. Am. Chem. Soc.* **1985**, *107*, 604−614. (b) Hashimoto, T.; Dyer, R. L.; Crossley, M. J.; Baldwin, J. E.; Basolo, F. B. *J. Am. Chem. Soc.* **1982**, *104*, 2101−2109. (c) Collman, J. P.; Brauman, J. I.; Fitzgerald, J. P.; Hampton, P. D.; Naruta, Y. P.; Sparapagny, J. W.; Ibers, J. A. *J. Am. Chem. Soc.* **1988**, *110*, 3477−3486. (d) Collman, J. P. *Acc. Chem Res.* **1977**, *10*, 265−772. (e) David, S.; James, B. R.; Dolphin, D.; Traylor, T. G.; Lopez, M. *J. Am. Chem. Soc.* **1994**, *116*, 6−14.

0020-1669/96/1335-2006$12.00/0 

using the Evans method[9] with TMS as the reference material. Visible spectra were measured with an Aminco DW2a or a Cary 2400 spectrophotometer typically in 1 cm Pyrex cuvettes thermostated at 25 °C.

**[Fe((DMG)$BPh_2$)$_2$]$_2$O.** Crystals of **1** formed over 24 h during the oxidation of a solution of Fe((DMG)$BPh_2$)$_2$($CH_3CN$)$_2$ (20 mg) in 3 mL of air-saturated acetone left in a capped vial. The black crystals were filtered out and washed with acetone. Yield: 10 mg (55%). Visible ($CH_2Cl_2$): 407 nm, $1.85 \times 10^4$ L mol$^{-1}$ cm$^{-1}$. $^1$H NMR ($CDCl_3$, $\delta$ (ppm)): DMG $CH_3$ 2.73, $Ph_{ax}$ ortho 6.55, $Ph_{ax}$ meta 6.73, $Ph_{ax}$ para 6.75, $Ph_{eq}$ para 7.22, $Ph_{eq}$ meta 7.28, $Ph_{eq}$ ortho 7.53. Magnetic moment (Evans method[9]) in $CDCl_3$: diamagnetic.

**[Fe((DMG)$BPh_2$)$_2$$BuNH_2$]$_2$O·2$CDCl_3$.** A blue solution of **2** was prepared by dissolving **1** (20 mg) in 1 mL of dry $CDCl_3$ and adding 25 $\mu$L of *n*-butylamine. This solution was layered with 1 mL of dry hexane and left capped with a serum cap in a desiccator for 3 days. The blue crystals were filtered out, and selected crystals were mounted immediately and coated with epoxy cement to prevent solvent loss. Visible ($CH_2Cl_2$): 706 nm, $1.2 \times 10^4$ L mol$^{-1}$ cm$^{-1}$. $^1$H NMR ($CDCl_3$, $\delta$ (ppm)): DMG $CH_3$ −4.16, $Ph_{ax}$ ortho 7.35, $Ph_{ax}$ meta 6.46, $Ph_{ax}$ para 6.29, $Ph_{eq}$ para 7.49, $Ph_{eq}$ meta 7.67, $Ph_{eq}$ ortho 8.04; $BuNH_2$ $\beta$-$CH_2$ −2.45, $\gamma$-$CH_2$ −0.23, $\delta$-$CH_3$ 0.81. Magnetic moment (Evans method[9]) in $CDCl_3$: $\mu = 2.9(1)$ $\mu_B$.

**Fe((DMG)$BPh_2$)$_2$−O−Fe((DMG)$BPh_2$)$_2$($BuNH_2$).** Solutions containing the monoligated species were generated in situ by addition of 1 equiv of $BuNH_2$ to **1**. Visible ($CH_2Cl_2$): $\lambda_{max}$ 475 nm. $^1$H NMR ($CDCl_3$, $\delta$ (ppm)): DMG $CH_3$ −7.92, +6.49; Ph 8.24, 7.91, 7.68, 7.6, 5.92, 5.74. 3.44; $BuNH_2$ $\beta$-$CH_2$ −2.54, $\gamma$-$CH_2$ −0.08, $\delta$-$CH_3$ +0.80. Magnetic moment: $\mu = 2.9(1)$ $\mu_B$.

**X-ray Crystallography.** All measurements were performed at room temperature on a Siemens R3m/V four-circle diffractometer using graphite-monochromatized Mo K$\alpha$ radiation ($\lambda = 0.710\,73$ Å). Cell parameters were determined by least-squares refinement of 25 high-angle reflections. Intensities of three standard reflections monitored every 97 reflections showed no decay. Structures were solved by direct or Patterson methods and Fourier expansion using the PC SHELXTL and SHELX93 software.[10] Final full-matrix least-squares refinement employed anisotropic thermal parameters for all non-hydrogen atoms with phenyls refined as rigid anisotropic groups. Hydrogen atoms were placed in idealized locations and refined with fixed isotropic thermal parameters (0.08) using a riding model. Absorption corrections based on $\psi$ scans were applied using the XEMP program. In **1**, 2-fold rotational symmetry is crystallographically imposed. Bond length constraints were applied to the two $CHCl_3$ solvent molecules in **2** (C−Cl = 1.77 Å), one of which (C(99)) was disordered. Crystallographic details are given in Table 1 and in the Supporting Information.

**Table 1.** Crystal Data and Data Collection Procedures

| | [Fe((DMG)$BPh_2$)$_2$]$_2$O (**1**) | [Fe((DMG)$BPh_2$)$_2$-$BuNH_2$]$_2$O·2$CHCl_3$ (**2**) |
|---|---|---|
| empirical formula | $Fe_2C_{64}H_{64}B_4N_8O_9$ | $Fe_2C_{74}H_{88}B_4N_{10}O_9Cl_6$ |
| fw | 1244.17 | 1629.18 |
| space group | *Pnna* | *P*1 |
| *a*, Å | 17.440(3) | 13.445(3) |
| *b*, Å | 21.381(4) | 14.525(4) |
| *c*, Å | 16.896(3) | 23.877(6) |
| α, deg | 90 | 96.01 |
| $\beta$, deg | 90 | 92.61 |
| $\gamma$, deg | 90 | 117.40(1) |
| *V*, Å$^3$ | 6300(2) | 4094(2) |
| *Z* | 4 | 2 |
| *d*(calc), g/mL | 1.312 | 1.322 |
| cryst shape | cube | thick plate |
| cryst dimens, mm | ca. 0.5 × 0.4 × 0.3 | ca. 0.8 × 0.3 × 0.15 |
| abs coeff, mm$^{-1}$ | 0.523 | 0.609 |
| scan type | $\theta/2\theta$ | $\theta/2\theta$ |
| scan range, deg | $3.5 \le 2\theta \le 50$ | $3.5 \le 2\theta \le 45$ |
| index ranges | $-1 \le h \le 20$ | $-1 \le h \le 14$ |
| | $-1 \le k \le 25$ | $-15 \le k \le 14$ |
| | $-1 \le l \le 20$ | $-25 \le l \le 25$ |
| tot. no. of reflcns | 6745 | 12 072 |
| tot. no. of unique reflns | 5559, $R_{int} = 0.0432$ | 10 480, $R_{int} = 0.0498$ |
| refinement method | full-matrix least-squares on $F^2$ | |
| data/restraints/params | 5555/0/345 | 10 423/18/878 |
| GOF on $F^2$ | 1.036 | 1.049 |
| final $R$ ($R_w^2$) [$I > 4\sigma$] | 0.0680 (0.1487) | 0.0861 (0.1983) |
| $R$ for all data | 0.1437 (0.1912) | 0.1693 (0.2869) |
| largest diff peak and hole, e/Å$^3$ | 0.470 and −0.302 | 0.657 and −0.576 |

## Results and Discussion

The oxo-bridged complexes are prepared by aerobic oxidation of the labile acetonitrile complex. The Fe((DMG)$BPh_2$)$_2$($CH_3CN$)$_2$ complex is air stable in the presence of excess $CH_3CN$ but oxidizes rapidily in air when dissolved in noncoordinating solvents (acetone, $CH_2Cl_2$), producing yellow-brown solutions of an EPR-silent oxo−diiron species. The unligated dimer, **1**, has a visible maximum at 407 nm in dry $CH_2Cl_2$. Addition of 1 equiv of $BuNH_2$ produces a monoligated species absorbing at 475 nm. Adding 2 equiv gives a blue diligated complex, **2**, with a characteristic intense band at 680 nm assigned to an oxo to iron charge transfer. Equilibrium constants and spectral data (visible and NMR) for a wide variety of half and fully ligated derivatives are presented elsewhere.[6i]

Solution magnetic measurements show diamagnetism (or at best very weak paramagnetism) for **1**. Magnetic moments of 2.9(1) $\mu_B$ are found for both the mono and bis $BuNH_2$ complexes. These are consistent with the spin-only moment for a triplet ground state. The diamagnetism for **1** is unique. It seems that the bending of the Fe−O−Fe bridge lifts the degeneracy of the $\pi$* HOMO, resulting in a singlet ground state. A more detailed discussion must await solid state magnetic measurements. The magnetic moments found for the ligated $\mu$-oxo species are similar to those reported for $\mu$-oxo ruthenium bipyridyl[11] and FePc systems[5] (both low-spin $d^5$). A metal−metal-bonded [RuTPP]$_2$, another example of an $S = 1$ system with $\pi$ symmetry has a reported magnetic moment of 2.8 $\mu_B$.[12]

**X-ray Structural Results.** The $\mu$-oxo $BPh_2$ complexes are analogous to $BF_2$ complexes described previously,[6d] but they are much more sluggish oxidants and do not revert to Fe(II) as rapidly. We have succeeded in growing X-ray-quality crystals of the pentacoordinate species and its butylamine adduct.

The structures of the unligated dimer **1** and butylamine derivative **2** are shown in Figures 1 and 2. In these oxo-bridged species, the macrocycle must adopt the $C_{2v}$ conformation in which both axial phenyls are directed toward the distal face (trans to the oxo bridge). This creates a cyclophane-like distal binding environment wherein ligation may be profoundly influenced by nonbonded contacts with the phenyl faces. Before we address these features, we first examine the primary structural features of the iron coordination sphere which provide evidence concerning the spin state of the irons.[13]

(9) (a) Evans, D. F.; James, T. A. *J. Chem. Soc., Dalton Trans.* **1979**, 723. (b) Sur, S. K. *J. Magn. Reson.* **1989**, *82*, 169−173.
(10) Sheldrick, G. M. *SHELXTL*, PC Version 4.1, and *SHELXL93*, PC Version; Siemens Analytical X-Ray Instruments Inc.: Madison, WI, 1993.
(11) Weaver, T. R.; Meyer, T. J.; Adeyemi, S. A.; Brown, G. M.; Eckberg, R. P.; Hatfield, W. E.; Johnson, E. C.; Murray, R. W.; Untereker, D. *J. Am. Chem. Soc.* **1975**, *97*, 3039−3048.
(12) Collman, J. P.; Barnes, C. E.; Swepston, P. N.; Ibers, J. A. *J. Am. Chem. Soc.* **1984**, *106*, 3500−3510.
(13) Spin state and structure have received considerable attention for hemes. (a) Scheidt, W. R.; Gouterman, M. In *Iron Porphyrins*; Lever, A. B. P., Gray, H. B., Eds.; Addison Wesley: Reading, MA, 1983; Part I, pp 89−140. (b) Scheidt, W. R.; Reed, C. A. *Chem. Rev.* **1981**, *81*, 543−55.
(14) Vogt, L. H.; Zalkin, A.; Templeton, D. H. *Inorg. Chem.* **1967**, *6*, 1725−1730.

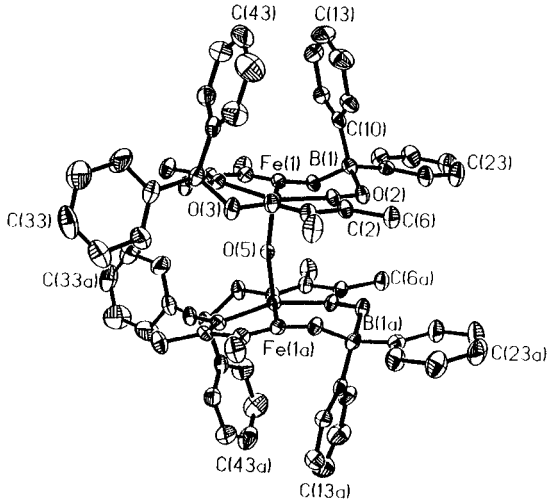


**Figure 1.** Structure of **1** = $[Fe((DMG)BPh_2)_2]_2O$ with 30% probability ellipsoids.

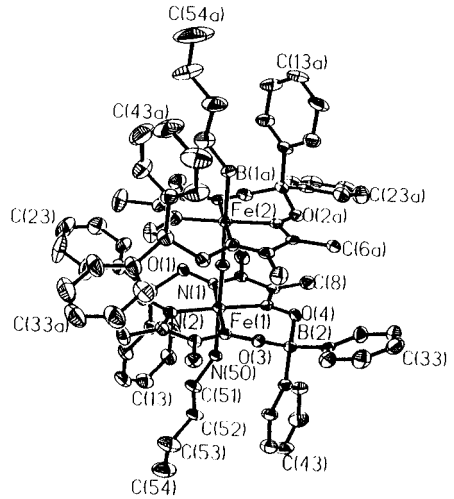


**Figure 2.** Structure of **2** = $[(BuNH_2)Fe((DMG)BPh_2)_2]_2O$ with 30% probability ellipsoids.

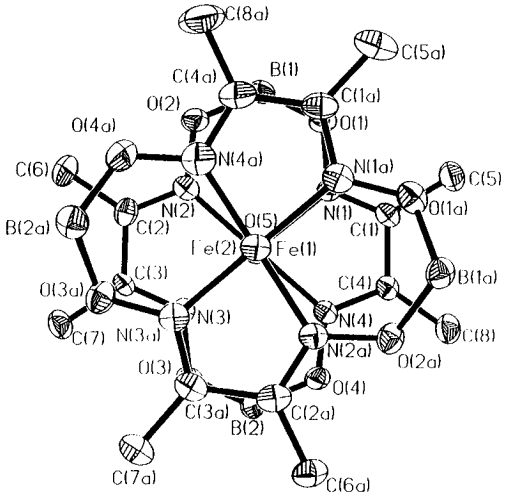


**Figure 3.** Geometry in **2** as viewed down the Fe−O−Fe axis with $BuNH_2$ and phenyl groups removed.

**Coordination Geometry.** The two $FeN_4$ fragments are mutually rotated by ∼90° in both **1** and **2**, which minimizes the phenyl−phenyl contacts and eclipses the Fe−N bonds (Figure 3). The staggered geometry is a common feature of oxo-bridged species[1−3] although one example of a nearly eclipsed heme $\mu$-oxo complex was reported recently.[15]

**Table 2.** Selected Bond Lengths (Å) for **1** and **2**

| bond | **1** | **2** |
|---|---|---|
| Fe(1)−O(5) | 1.7097(10) | 1.766(6) |
| Fe(2)−O(5) | 1.7097(10) | 1.764(6) |
| Fe(1)−N(1) | 1.910(4) | 1.894(7) |
| Fe(1)−N(2) | 1.905(4) | 1.883(7) |
| Fe(1)−N(3) | 1.916(4) | 1.895(7) |
| Fe(1)−N(4) | 1.908(4) | 1.891(7) |
| N(1)−C(1) | 1.282(6) | 1.277(10) |
| N(1)−O(1) | 1.363(5) | 1.371(9) |
| N(2)−C(2) | 1.297(6) | 1.293(11) |
| N(2)−O(2) | 1.359(5) | 1.357(9) |
| N(3)−C(3) | 1.292(7) | 1.296(10) |
| N(3)−O(3) | 1.362(5) | 1.360(9) |
| N(4)−C(4) | 1.311(6) | 1.320(10) |
| N(4)−O(4) | 1.350(5) | 1.357(9) |
| O(1)−B(1) | 1.546(7) | 1.526(12) |
| O(2)−B(1) | 1.526(7) | 1.540(12) |
| O(3)−B(2) | 1.552(8) | 1.520(12) |
| O(4)−B(2) | 1.535(7) | 1.536(12) |
| B(1)−C(10) | 1.627(8) | 1.640(13) |
| B(1)−C(20) | 1.616(7) | 1.615(12) |
| B(2)−C(30) | 1.613(7) | 1.621(12) |
| B(2)−C(40) | 1.598(8) | 1.658(11) |
| C(1)−C(4) | 1.474(7) | 1.479(12) |
| C(2)−C(3) | 1.471(7) | 1.464(13) |
| Fe(1)−N(50) | | 2.070(7) |
| N(50)−C(51) | | 1.494(11) |
| C(51)−C(52) | | 1.526(13) |
| C(52)−C(53) | | 1.56(2) |
| C(53)−C(54) | | 1.46(2) |

**Table 3.** Comparative Structural Data for ($\mu$-Oxo)diiron(III) Complexes

| | Fe−$N_4$,[a] Å | Fe−O, Å | FeOFe, deg | Fe−Ct,[c] Å | ref[d] |
|---|---|---|---|---|---|
| **1** | 1.91 | 1.709 | 166.0 | 0.30 | *b* |
| **2** | 1.89 | 1.766 | 178.6 | 0.026 | *b* |
| $[FePc(MeIm)]_2O$ | 1.92 | 1.749 | 175.1 | 0.02 | 5b |
| $[MnPc(PY)]_2O$ | 1.97 | 1.71 | 178 | 0.0 | 14 |
| $[Fe(salen)]_2)O$ | | 1.78 | 144.6 | 0.58 | 3c |
| $[Fe(3\text{-}tbusaltmen)]_2O$ | | 1.779 | 173.4 | 0.62 | 3a |
| $[Fe(acen)]_2O$ | | 1.775 | 150.7 | 0.58 | 3b |
| $[Fe(TPP)]_2O$ | 2.087 | 1.763 | 174.5 | 0.50 | 2a |
| $Fe_2(\mu\text{-}O)FF$ | 2.075 | 1.792 | 161.4 | 0.62 | 2b |
| $[Fe(Cl_3)]_2O^{2-}$ | | 1.74−1.77 | 146−180 | | 1d |
| 36 supported | | 1.86−2.1 | 98−130 | | 4 |

[a] Average Fe−N bond length in the $N_4$ plane. [b] This work. [c] Displacement of Fe from the $N_4$ plane. [d] See ref 1b for a more extensive tabulation of $\mu$-oxo structures.

The ligated species, **2**, shows metrical features consistent with a low-spin Fe(III) with an average Fe−$N_4$ distance of 1.89 Å and the iron essentially in the $N_4$ plane. The structure resembles closely that for the low-spin $[FePc(MeIM)]_2O$ complex[5] and a manganese analogue[14] shown in Table 3.

In the unligated species, the iron is 0.3 Å out of the $N_4$ plane with average Fe−N bond lengths of 1.91 Å. These features also suggest a low-spin state. The high-spin heme, Schiff base, and other oxo diiron systems give significantly greater radial expansion ($FeN_4$) and almost twice the displacement from the $N_4$ plane. While the Fe−$N_4$ bond lengths are also consistent with an intermediate-spin state[13] for **1**, the short Fe−O bond is not. The Fe−O bond in **1** is the shortest known iron−$\mu$-oxo bond length! Even the longer Fe−O bonds in **2** fall at the low end of the range typically found for oxo−iron bonds in Table 3.

**The Distal Binding Cavity in 2.** The butylamine ligand in **2** is sandwiched between two axial phenyls, and as a conse-

(15) Cheng, B.; Hobbs, J. D.; Debrunner, P. G.; Erlebacher, J.; Shelnutt, J. A.; Schedit, W. R. *Inorg. Chem.* **1995**, *34*, 102−110.

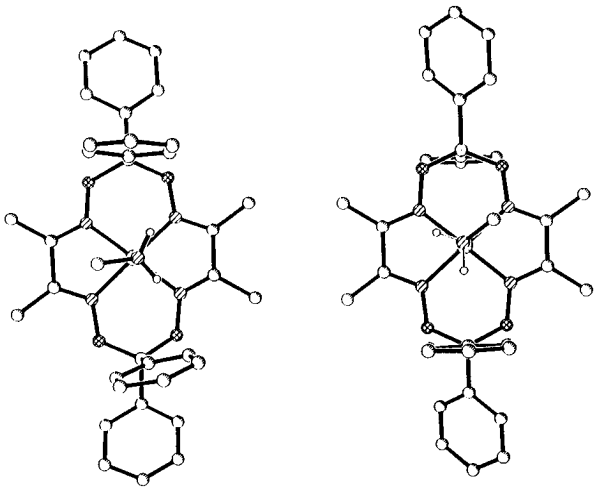

**Figure 4.** Axial views showing the orientation of the $NH_2$ and α-carbon of the bound $BuNH_2$ ligand in **2** and in $Fe((DMG)BPh_2)_2(BuNH_2)_2$. Other atoms in the $BuNH_2$ ligand are omitted.

quence the butylamine backbone is nearly flat. The $NH_2$ group is oriented with one N−H directed toward each of the two axial phenyl faces with the hydrogens 2.6 Å above the phenyl rings. This orientation is compared in Figure 4 with that found for $Fe((DMG)BPh_2)_2(BuNH_2)_2$ in which only a single axial phenyl lies adjacent to the binding site.[6h] In the Fe(II) complex, the one N−H bond projects toward the face of a single phenyl leaving the α-carbon to point away. The favored orientation of the $BuNH_2$ substrate appears to maximize N−H $\pi$ attractive forces[16] and perhaps more importantly minimize Ph−butyl repulsions in the two cases shown. The Fe−N bond length of 2.070(7) Å is only slightly longer than that found for the low-spin Fe(II) bis(butylamine) complex (2.053 Å).[6h]

**Superstructural Effects.** Interactions between a host superstructure and the substrate binding within it are of intense current interest.[17−19] Attention has focused on the importance of preorganization of the host and the significance, if any, of postorganization (conformational changes in the host required in order for it to accommodate specific guests), as well as specific interactions between the host and guest which might contribute to the binding energetics.

The cyclophane-like environment surrounding the $BuNH_2$ ligand in **2** is also found in the structures of several Fe(II) derivatives where ligands (L) are bound between the two axial phenyls and a pyridine occupies the trans site. The X-ray structural data for $Fe((DMG)BPh_2)_2(PY)L$, L = TCNE, PY, $NH_3$, CO, are reported elsewhere.[6i] In these structures the iron displacement from the $N_4$ plane (0.04−0.08 Å) is always toward the ligand on the superstructured face while in **2** the displacement lies toward the oxo group. This shows that the iron position is not imposed solely by the demands of the $N_4$ ligand in its $C_{2v}$ conformation.

The oxo-bridged complexes **1** and **2** reveal several significant superstructural changes in response to ligation. The distal cavity

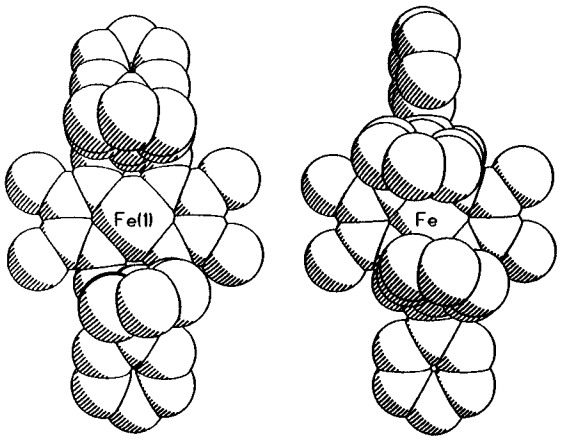


**Figure 5.** Space-filling views of the distal binding cavity in **1** (right) and **2** (left). The $BuNH_2$ ligand in **2** has been omitted to reveal the cavity size.

in **1** has undergone a significant collapse in comparison with that in **2** (Figure 5). Such cavity collapses are found in capped hemes,[17] in the lacunar systems studied by Busch,[18] and in host−guest systems.[19] In **1**, one axial phenyl protrudes into the cavity more than the other. This asymmetry is evident in the different displacements of B(1) and B(2) from the $N_4$ plane (0.58 and 0.71 Å, respectively) and in Figure 5, where the para carbons of the two axial phenyls are displaced to opposite sides of a vertical plane through B(1), Fe, and B(2). The collapse of the cyclophane cavity serves to partially fill the void above the vacant binding site. These distortions reflect the natural tendency for axial groups to pinch inward in six-membered chelate rings (see for example the structure for $Fe((DMG)BF_2)_2(PY)(CO)$[6h]). The pinching or collapse in **1** is much greater because no ligand opposes it and because the Fe atom is displaced toward the opposite face. The distortion is asymmetric in **1** in order to avoid para-carbon contacts of the two axial phenyls.

This is the first example of a pentacoordinate iron dioxime, and therefore it provides a useful model for the reactive intermediate in the dissociative ligand substitution reactions of Fe(II) dioxime complexes.[20] The cavity collapse found in **1** supports our previous predictions[6e] for the pentacoordinate structure based upon the unusual on-rate discrimination in CO binding to $Fe((DMG)BPh_2)_2(PY)_2$.

The bend of the Fe−O−Fe bridge causes the two $N_4$ planes to tilt at an angle of 12°, increasing the interplanar separation along one edge and decreasing it along the opposite edge. The different orientations of the equatorial phenyls seen in Figures 1 and 2 are related to changes accompanying the bend of the Fe−O−Fe unit and to the collapse of the distal cavity. All four equatorial phenyls in **2** lie approximately parallel to the $N_4$ planes dipping slightly downward to flank the oxo cavity. In **1** the equatorial phenyls flanking the more exposed edge are almost perpendicular to the $N_4$ planes allowing the ortho C−H groups to protude into the more exposed side of the oxo cavity. The equatorial phenyls flanking the opposite edge remain approximately coplanar with the $N_4$ planes, much as they are found in **2**.

While the Fe−O bonds are shorter in **1**, the distance between the $N_4$ units (measured from their centers) is significantly longer (3.588 Å in **2** and 3.983 Å in **1**) because of the position of the irons out of the $N_4$ plane toward the oxygen. This coupled with the bending and tilting leaves the oxo group more exposed in **1** than it is in **2** (Figure 6).

(16) Nishio, M.; Hirota, M. *Tetrahedron* **1989**, *45*, 7201−7245.
(17) (a) Slebodnik, C.; Kim, K.; Ibers, J. A. *Inorg. Chem.* **1993**, *32*, 5338−5342. (b) Imai, H.; Nakagawa, S.; Kyuno, E. *J. Am. Chem. Soc.* **1992**, *114*, 6719−6723.
(18) (a) Alcock, N. W.; Lin, W.; Cairns, C.; Pike, G. A.; Busch, D. H. *J. Am. Chem. Soc.* **1989**, *111*, 6630−6643. (b) Lin, W.; Alcock, N.; Busch, D. H. *J. Am. Chem. Soc.* **1991**, *113*, 7603−7608. (c) Herron, H.; Zimmer, L. L.; Gryzbowski, J. J.; Olszanski, D. J.; Jackels, S. C.; Callahan, R. W.; Cameron, J. H.; Christoph, G. G.; Busch, D. H. *J. Am. Chem. Soc.* **1983**, *105*, 6585. (d) Busch, D. H.; Stephenson, N. A. *Coord. Chem Rev.* **1990**, *100*, 119.
(19) Robbins, T. A.; Knobler, C. B.; Cram, D. J. *J. Am. Chem. Soc.* **1994**, *116*, 111−122.
(20) Chen, X.; Stynes, D. V. *Inorg. Chem.* **1986**, *25*, 1173−1182.

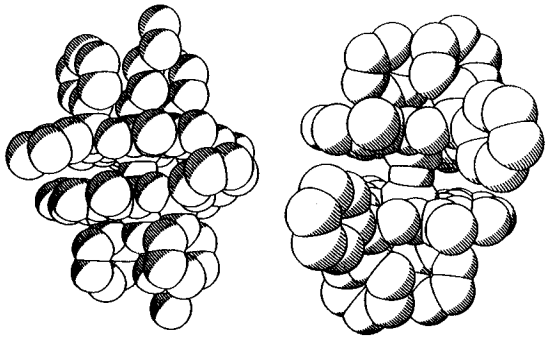

**Figure 6.** Views into the proximal cavity in **1** (right) and **2** (left) showing greater exposure of the oxo group in **1**.

**Comparisons with Hemes and Hemoproteins.** The contrast in the ligation and spin state of these $\mu$-oxo systems compared with hemes is worth noting. No heme $\mu$-oxo complex shows any evidence for ligation (even in neat pyridine), and all have a similar high-spin geometry. The dioxime-derived iron macrocycles also show dramatic differences from hemes and Schiff base systems in the greater inertness of their Fe(II) complexes[6a,17] and much greater oxidizing strength of their Fe(III) derivatives.[6a] These features are explained on the basis of the greater $\pi$-acceptor character of the dioximes. Most of the macrocycle's $-2$ formal charge is located away from the ligand donor atoms (and the iron) in the dioximato systems. This permits more extensive delocalization of (*xz*,*yz*) onto the $N_4$ ligand, thus reducing repulsion of axial ligands. The observation of pentacoordination in **1** may be partly a consequence of the trans effect of the oxo group. Trans labilizations as large as $10^5$ have been noted in $Fe^{II}((DMG)BF_2)_2$ complexes containing $\pi$-donor halide ligands.[21]

There are several similarities in the structural changes accompanying ligation to **1** and those which occur on ligation to hemoglobin.[22] Both show a collapse of peripheral groups (HIS E7 and VAL E11 in Hb) which partially block access to the vacant site. Both involve significant movement of the iron vis-à-vis the $N_4$ plane, and both reveal major structural reorganization of the peripheral environments on both sides of the $FeN_4$ plane brought about as a result of ligation.

In hemoglobin, these changes form part of the structural basis for its cooperativity which derives from a 2−3 kcal/mol difference in the free energy for $O_2$ ligation to T vs R state Hb.[23] Studies of ligation to **1** reveal a negative cooperativity for pyridine binding. A difference of 6 kcal/mol is found in ligation free energy in the two ligation steps.[24] The negative cooperativity is thought to result from the transmission of strain initiated by the ligand-induced opening of the cyclophane cavity. This coupled with the movement the iron into the $N_4$ plane can lead to interfacial contacts which restrict the corresponding structural changes at the remote site. Details of these effects and their dependence on the nature of the axial ligand are described in a subsequent paper.[6i]

The role (if any) of conformationally mobile fragments located near binding sites whether in proteins[25] or in structurally elaborate models cannot be established from structural data alone. Some close contacts look important but are not. Others which seem relatively inocuous can have a profound effect on binding energetics. In hemoproteins, the reported bending or tilting of CO looks significant but seems not to be a factor in the binding energetics.[26] In contrast, much more subtle variations in structure sometimes distant from the binding site can have profound consequences.[27] The relative locations of molecular fragments are obvious in structures, but the energetics involved in moving these fragments and the Coulombic forces between them are not. This is one of the problems which the study of structurally elaborate model systems seeks to address.

**Acknowledgment.** We thank the NSERC of Canada for financial support and York University for funding the X-ray diffraction facility.

**Supporting Information Available:** Complete listings of atomic coordinates, thermal parameters, bond lengths and angles, and hydrogen atom positions for **1** and **2** (15 pages). This material is available in many libraries on microfiche, immediately follows this article in the microfilm version of the journal, and can be ordered from ACS; see any current masthead page for ordering information.

IC950801G

(21) de Silva, D. G. A. H.; Thompson, D. W.; Stynes, D. V. *Inorg. Chem.* **1991**, *30*, 4856−4858.
(22) Baldwin, J.; Chothia, C. *J. Mol. Biol.* **1979**, *129*, 175−220.
(23) MacQuarrie, R.; Gibson, Q. H. *J. Biol. Chem.* **1971**, *246*, 5832.
(24) Stepwise binding constants for pyridine in $CH_2Cl_2$ at 25 °C: $BPh_2$, log $K_1 = 3.8$, log $K_2 = -0.7$; $BF_2$ system, log $K_1$ and log $K_2 > 4$.[6i]
(25) Case, D. A.; Karplus, M. *J. Mol. Biol.* **1979**, *132*, 343−368.
(26) (a) Traylor, T. G.; Tsuchiya, S.; Campbell, D.; Mitchell, M.; Stynes, D. V.; Koga, N. *J. Am. Chem. Soc.* **1985**, *107*, 604−614. (b) Ray, G. B.; Li, X.; Ibers, J. A.; Sessler, J. L.; Spiro, T. G. *J. Am. Chem. Soc.* **1994**, *116*, 162−176. (c) Lim, M.; Jackson, T. A.; Anfinrud, P. A. *Science* **1995**, *269*, 962−966.
(27) Antonini, E.; Brunori, M. *Hemoglobin and Myoglobin in their Reactions with Ligands;* North Holland: Amsterdam, 1971.